Recent achievements towards aero-structure gradient computation using high-fidelity CFD-CSM in the Onera ELSA software

Christophe Blondeau, Timothée Achard, Philippe Girodroux-Lavigne, Roger Ohayon

RECENT ACHIEVEMENTS TOWARDS AERO-STRUCTURE GRADIENT COMPUTATION USING HIGH-FIDELITY CFD-CSM IN THE ONERA ELSA SOFTWARE

C. Blondeau[1†], T. Achard[1‡], P. Girodroux-Lavigne[1†], R. Ohayon[2§]

[1]ONERA BP72 – 29 avenue de la Division Leclerc, FR-92322 CHATILLON CEDEX
Christophe.Blondeau@onera.fr

[2]CNAM – 2 rue Conté, FR-75003 PARIS
Roger.Ohayon@cnam.fr

Keywords: optimization, aeroelastic gradient, adjoint technique.

Abstract: Strategies for developing and implementing discrete gradient methods for aeroelastic optimization for structured meshes are presented. For shape optimization of aerodynamic functions, discrete linear and adjoint techniques taking into account structural flexibility are introduced. To this end, all routines of the block-structured ***elsA***/Aeroelastic solver have been systematically differentiated by hand. All operations are performed on-the-fly for linear and tangent mode without any data storage or transposing thus leading to a very memory efficient implementation. These techniques are demonstrated on a flexible gradient computation exercise for the Onera M6 wing. Comparisons between rigid and flexible gradients are presented for Euler and Navier-stokes fluid. A second part of this paper presents a non-intrusive strategy for the computation of flexible gradients with respect to structural design parameters. To this end, a modal projection technique associated to a linearized frequency response solver is proposed. Alternatives to reduce the associated computational overhead are discussed. An illustration of this approach is presented for the M6 wing Euler test case.

1 INTRODUCTION

Design of aeroelastic and aerodynamic performance has benefited not only from recent achievements in terms of numerical tools for computation of flexible gradients through tangent or adjoint approach but also from the re-organization of the optimization process itself to deal with high-fidelity aerodynamic and structural models [1, 2].
It is now recognized that rigid aerodynamic shape optimization for drag reduction has to consider the impact of structural flexibility on the performance especially in the context of multi-point optimization. On the other hand, aeroelastic design (i.e. structural weight optimization by tailoring static or dynamic aeroelastic loads) has evolved towards CFD modelling for flexible loads prediction [1].
This paper presents the latest achievements about the development of a high-fidelity based aero-structure gradient computation capability in the framework of the ***elsA*** software [3, 4].

---

† Research scientist, Aeroelasticity and Structural Dynamics Department, ONERA.
‡ Phd candidate, Ecole doctorale Sciences et Métiers de l'Ingénieur (SMI) - ED432, CNAM Paris.
§ Professor, Structural Mechanics and Coupled Systems Laboratory, CNAM Paris

By aero-structure we mean gradient of any function of interest with respect to aerodynamic shape or structural design parameters.
Up to now, structural modelling for flexible gradient computation was limited to a beam-like equivalent model for the wing box [5]. More recently this approach was extended to get sensitivities of an aerodynamic function of interest (drag component, lift coefficient, L/D ratio …) with respect to structural design parameters such as wall thicknesses of skins and spars for an ideal rectangular wing section, but still limited to an equivalent beam model kinematics [6, 7].
Although useful for preliminary design studies and design space exploration, this structural modelling is not able to tackle complex aeroelastic couplings, nor deal with composite structures for efficient aeroelastic tailoring design, and is obviously limited to large aspect ratio wings.
The objective of the present work was to relief all these limitations by re-developing an aero-structure gradient capability from scratch by systematic differentiation of discretized aero-elastic equations, and all associated operators, in the ***elsA*** aeroelasticity module (***elsA***/Ael). This way, the new capability inherits the structural paradigm embedded into the ***elsA***/Ael module (structural flexibility matrix), the whole catalogue of fluid-structure transfer methods, as well as the underlying parallel architecture. High-fidelity aero-structure gradient computations and optimization studies using the adjoint approach have been reported in the literature for structured and unstructured grids [8-12]. However, none of them seems to have a core memory efficient on-the-fly implementation for deriving algebra manipulations such as matrix-vector product involving the geometric or state residual Jacobian matrix.
In the following, equations and solving procedure for the aeroelastic gradient are discussed as well as the numerical control parameters and their impact on the solution convergence.
Preliminary results for static aeroelastic gradient computations with respect to aerodynamic shape parameters, in linear and adjoint mode, for the Onera M6 wing will be presented. Euler and RANS fluid modelling will be considered.
On going extension work of the aeroelastic gradient tool in order to consider structural variables will also be presented. Two approaches can be considered. The first one, called intrusive approach, needs a substantial modification of the ***elsA*** source code. The second one, called non-intrusive, considers a projection of the static displacement field on the structural mode shapes in order to benefit from the classical harmonic forced response mode of linearized Euler or RANS simulation tools. Preliminary results for this second approach will be presented for the Onera M6 wing with respect to stiffness parameters of the primary wing box structure.

2 SENSITIVITY OF A STRONGLY COUPLED AEROELASTIC SYSTEM

In order to introduce notations and remind typical solving techniques, a brief review of sensitivity analysis methods for aerodynamic and structural systems of discretized equations is given first. The interested reader should refer to [13] for a complete review of numerical sensitivity analysis.

As the subsequent derivations will always be related to discretized equations, it will not be reminded elsewhere in the following discussion. The generalization to a strongly coupled fluid-structure system will then be presented. The subsequent derivations are valid for any set of design parameters (i.e. impacting local aerodynamic shape only, structural stiffness only or both aerodynamic shape and stiffness as global design variables).

2.1 Gradient evaluation for a mono-disciplinary system

Any discretized set of steady-state nonlinear equilibrium equations can be written in the following residual form

$$\mathbf{R}(\mathbf{p}, \mathbf{y}(\mathbf{p})) = \mathbf{0} \tag{1}$$

Where $\mathbf{p}$ and $\mathbf{y}(\mathbf{p})$ represent the vector of n_p design variables and the corresponding dependent state vector. $\mathbf{R}$ represents either a second-order accurate cell-centered finite volume spatial discretization of the fluid residual or a finite element spatial discretization of the structural residual. Note that Eq. (1) has an implicit dependency on the computational aerodynamic grid $\mathbf{X}_a(\mathbf{p})$ or structural grid $\mathbf{X}_s(\mathbf{p})$. To simplify notations, this dependency is only reproduced when necessary in subsequent expressions. $\mathbf{R}$ is supposed to be once continuously differentiable with respect to the state variables and computational mesh in the vicinity of $\mathbf{y}(\mathbf{p})$ and $\mathbf{X}(\mathbf{p})$.

We are interested in the sensitivity derivatives of any set of function $\mathbf{f} = \mathbf{f}(\mathbf{p}, \mathbf{y}(\mathbf{p}))$ with respect to a design variable. Applying the chain rule differentiation to $\mathbf{f}$ yields:

$$\frac{\mathrm{d}\mathbf{f}}{\mathrm{d}\mathbf{p}} = \frac{\partial \mathbf{f}}{\partial \mathbf{p}} + \frac{\partial \mathbf{f}}{\partial \mathbf{y}} \frac{\mathrm{d}\mathbf{y}}{\mathrm{d}\mathbf{p}} \tag{2}$$

The total sensitivity derivatives $\mathrm{d}\mathbf{y}/\mathrm{d}\mathbf{p}$ are computed from the differentiation of the discrete residual Eq. (1)

$$\frac{\mathrm{d}\mathbf{R}\left(\mathbf{p}, \mathbf{y}(\mathbf{p})\right)}{\mathrm{d}\mathbf{p}} = \frac{\partial \mathbf{R}}{\partial \mathbf{p}} + \frac{\partial \mathbf{R}}{\partial \mathbf{y}} \frac{\mathrm{d}\mathbf{y}}{\mathrm{d}\mathbf{p}} = \mathbf{0} \Rightarrow \frac{\mathrm{d}\mathbf{y}}{\mathrm{d}\mathbf{p}} = -\left[\frac{\partial \mathbf{R}}{\partial \mathbf{y}}\right]^{-1} \frac{\partial \mathbf{R}}{\partial \mathbf{p}} \tag{3}$$

where the Jacobian matrix $\partial \mathbf{R}/\partial \mathbf{y}$ is assumed invertible. Note that the gradient vanishes because the residual equation has to be satisfied for any value of $\mathbf{p}$. Usually terms like $\partial \boldsymbol{f}/\partial \mathbf{p}$, $\partial \boldsymbol{f}/\partial \mathbf{y}$ or $\partial \mathbf{R}/\partial \mathbf{p}$ are obtained analytically (full differentiation by hand) or numerically (automatic differentiation, finite differences or complex step).

Adjoint equations for a scalar function of interest are derived from Eq. (2) by substituting for $\mathrm{d}\mathbf{y}/\mathrm{d}\boldsymbol{p}$ from Eq. (3) to obtain

$$\frac{\mathrm{d}f}{\mathrm{d}\mathbf{p}} = \frac{\partial f}{\partial \mathbf{p}} + \mathbf{\Lambda}^T \frac{\partial \mathbf{R}}{\partial \mathbf{p}} \tag{4}$$

where $\mathbf{\Lambda}$ is a vector of adjoint variables that satisfies

$$\left[\frac{\partial \mathbf{R}}{\partial \mathbf{y}}\right]^T \mathbf{\Lambda} = -\frac{\partial f^T}{\partial \mathbf{y}} \tag{5}$$

This expression is independent of the design variables $\mathbf{p}$, which makes it particularly attractive for aerodynamic optimization problems with a large number of design parameters and relatively few responses of interest.

Considering an aerodynamic problem Eq. (1) is a system of n_w nonlinear equations with n_w unknowns. As an example, let's consider the functional dependency of a drag coefficient with respect to a set of shape design parameters:

$$C_D = F(\mathbf{W}(\mathbf{p}), \mathbf{X}_a(\mathbf{p})) = F(F_3(F_2(F_1(\mathbf{p})))) \tag{6}$$

where $\mathbf{W}$ represents the fluid conservative variables. Functional F_1 is the surface mesh parameterization that links design parameters to wetted surface grid positions. F_2 is the volumic mesh deformation operator that propagates the surface displacements to the interior fluid domain: $\mathbf{X}_a = F_2(\mathbf{X}_{surf})$. The fluid states $\mathbf{W} = F_3(\mathbf{X}_{vol})$ are obtained by solving the discretized fluid equations under prescribed boundary conditions. Eq. (6) exhibits an additional direct dependency to the grid $\mathbf{X}_a$ and is thus a generalization of Eq. (1). Direct differentiation of Eq. (6) wrt. $\mathbf{p}$ gives

$$\frac{\mathrm{d}C_D}{\mathrm{d}\mathbf{p}} = \frac{\partial C_D}{\partial \mathbf{W}}\frac{\mathrm{d}\mathbf{W}}{\mathrm{d}\mathbf{p}} + \frac{\partial C_D}{\partial \mathbf{X}_a}\frac{\partial \mathbf{X}_a}{\partial \mathbf{X}_{surf}}\frac{\mathrm{d}\mathbf{X}_{surf}}{\mathrm{d}\mathbf{p}} \tag{7}$$

Then differentiating the discrete residual $\mathbf{R}(\mathbf{W}, \mathbf{X}_a)$ wrt. $\mathbf{p}$ leads to the following expression for the total derivatives of the fluid states:

$$\frac{\mathrm{d}\mathbf{R}(\mathbf{W}, \mathbf{X}_a)}{\mathrm{d}\mathbf{p}} = \frac{\partial \mathbf{R}}{\partial \mathbf{W}}\frac{\mathrm{d}\mathbf{W}}{\mathrm{d}\mathbf{p}} + \frac{\partial \mathbf{R}}{\partial \mathbf{X}_a}\frac{\mathrm{d}\mathbf{X}_a}{\mathrm{d}\mathbf{p}} = \mathbf{0} \Rightarrow \frac{\mathrm{d}\mathbf{W}}{\mathrm{d}\mathbf{p}} = -\left[\frac{\partial \mathbf{R}}{\partial \mathbf{W}}\right]^{-1}\frac{\mathrm{d}\mathbf{R}}{\mathrm{d}\mathbf{p}} \tag{8}$$

Terms $\partial C_D / \partial \mathbf{W}$ and $\partial C_D / \partial \mathbf{X}_a$ are computed analytically around the equilibrium solution that satisfies $\mathbf{R}(\mathbf{W}, \mathbf{X}_a) = \mathbf{0}$.

The adjoint counterpart of Eq. (7) reads

$$\frac{\mathrm{d}C_D}{\mathrm{d}\mathbf{p}} = -\frac{\partial C_D}{\partial \mathbf{W}}\left[\frac{\partial \mathbf{R}}{\partial \mathbf{W}}\right]^{-1}\frac{\partial \mathbf{R}}{\partial \boldsymbol{p}} + \frac{\partial C_D}{\partial \mathbf{X}_a}\frac{\mathrm{d}\mathbf{X}_a}{\mathrm{d}\mathbf{p}} = -\boldsymbol{\Lambda}^T\frac{\partial \mathbf{R}}{\partial \mathbf{p}} + \frac{\partial C_D}{\partial \mathbf{X}_a}\frac{\mathrm{d}\mathbf{X}_a}{\mathrm{d}\mathbf{p}} \tag{9}$$

with $\boldsymbol{\Lambda}$ the vector of adjoint variables that satisfies

$$\left[\frac{\partial \mathbf{R}}{\partial \mathbf{W}}\right]^T \boldsymbol{\Lambda} = \frac{\partial C_D}{\partial \mathbf{W}}^T \tag{10}$$

A standard Backward Euler iterative scheme is used to solve for the static equilibrium. The discrete residual is linearized around the flow solution $\mathbf{W}^n$ at current iteration and a pseudo time step Δt is introduced along with a suitable approximation of the Jacobian matrix [14] to form the implicit term in the following preconditioned fixed point iterative scheme:

$$\left(\frac{\mathbf{I}}{\Delta t} + \frac{\partial \mathbf{R}}{\partial \mathbf{W}}^{app}\right)(\mathbf{W}^{n+1} - \mathbf{W}^n) = -\mathbf{R}(\mathbf{W}^n) \tag{11}$$

Applying this algorithm to the linearized form of the residual (around the steady state solution) in Eq. (8) gives the following iterative scheme for the total derivative of the flow field $\mathrm{d}\mathbf{W}/\mathrm{d}\mathbf{p}$:

$$\left[\frac{\mathbf{I}}{\Delta t}+\frac{\partial \mathbf{R}}{\partial \mathbf{W}}^{app}\right]\left(\frac{\mathrm{d}\mathbf{W}^{n+1}}{\mathrm{d}\mathbf{p}}-\frac{\mathrm{d}\mathbf{W}^{n}}{\mathrm{d}\boldsymbol{p}}\right)=-\frac{\partial \mathbf{R}}{\partial \mathbf{X}_a}\frac{\mathrm{d}\mathbf{X}_a}{\mathrm{d}\mathbf{p}}-\frac{\partial \mathbf{R}}{\partial \mathbf{W}}\frac{\mathrm{d}\mathbf{W}^{n}}{\mathrm{d}\mathbf{p}} \tag{12}$$

In a similar manner the iterative formula for the adjoint vector is derived,

$$\left[\frac{\mathbf{I}}{\Delta t}+\frac{\partial \mathbf{R}}{\partial \mathbf{W}}^{app}\right]^{T}(\boldsymbol{\Lambda}^{n+1}-\boldsymbol{\Lambda}^{n})=\frac{\partial {C_D}^{T}}{\partial \mathbf{W}}-\left[\frac{\partial \mathbf{R}}{\partial \mathbf{W}}\right]^{T}\boldsymbol{\Lambda}^{n} \tag{13}$$

Clearly expressions in Eq. (12) and (13) are very similar and it is straightforward to show that the following property holds

$$\boldsymbol{\Lambda}^{T}\frac{\partial \mathbf{R}}{\partial \mathbf{X}_a}\frac{\mathrm{d}\mathbf{X}_a}{\mathrm{d}\mathbf{p}}=-\frac{\partial {C_D}^{T}}{\partial \mathbf{W}}\frac{\mathrm{d}\mathbf{W}}{\mathrm{d}\mathbf{p}} \tag{14}$$

An exact dual algorithm has been proposed in [15] to enforce this property at every iteration.

Let's now consider the classical structural mechanics example of finding the total gradient of a constraint response in a finite element. The system is discretized by the finite element method to give the residual discrete system of equations

$$\mathbf{R}(\mathbf{U}(\mathbf{p}),\mathbf{X}_s(\mathbf{p}))=\mathbf{0}\Leftrightarrow\mathbf{K}(\mathbf{p})\mathbf{U}(\mathbf{p})-\mathbf{Q}(\mathbf{p})=\mathbf{0} \tag{15}$$

where $\mathbf{U}(\mathbf{p})$ and $\mathbf{Q}(\mathbf{p})$ represent the nodal displacements and the applied loads. The stiffness matrix $\mathbf{K}(\mathbf{p})$ is positive semi-definite and self-adjoint.

Assuming a general linear elastic behavior, the relationship between stresses and strains will be linear of the form $\boldsymbol{\sigma}=\mathbf{H}(\boldsymbol{\varepsilon}-\boldsymbol{\varepsilon}_0)+\boldsymbol{\sigma}_0$, where $\mathbf{H}$ denotes the elasticity matrix and $\boldsymbol{\varepsilon}_0$ and $\boldsymbol{\sigma}_0$ the initial strain and stress fields. The deformation field is obtained from the nodal displacements through the usual relation $\boldsymbol{\varepsilon}=\mathbf{S}\,\mathbf{N}\,\mathbf{U}(\mathbf{p})=\mathbf{B}\,\mathbf{U}(\mathbf{p})$, $\mathbf{S}$ being a linear differential operator and $\mathbf{N}$ the matrix of shape functions. Finally the constraint function reads

$$\boldsymbol{\sigma}=\mathbf{H}\,\mathbf{B}\,\mathbf{U}(\mathbf{p},\mathbf{X}_s(\mathbf{p}))-\mathbf{H}\boldsymbol{\varepsilon}_0+\boldsymbol{\sigma}_0 \tag{16}$$

Direct differentiation of Eq. (16) wrt. a scalar parameter p yields

$$\frac{\mathrm{d}\boldsymbol{\sigma}}{\mathrm{d}p}=\frac{\partial\boldsymbol{\sigma}}{\partial\mathbf{U}}\frac{\mathrm{d}\mathbf{U}}{\mathrm{d}p}=\mathbf{H}\,\mathbf{B}\frac{\mathrm{d}\mathbf{U}}{\mathrm{d}p}=\mathbf{H}\,\mathbf{B}\left(\frac{\partial\mathbf{U}}{\partial p}+\frac{\partial\mathbf{U}}{\partial\mathbf{X}_s}\frac{\mathrm{d}\mathbf{X}_s}{\mathrm{d}p}\right) \tag{17}$$

In the above expressions the geometric dependency of the structural mesh to the design parameter has been emphasized. Once again, for sake of clarity and without any loss of generality it will be omitted in the following when necessary.

From Eq. (15) direct differentiation gives

$$\frac{\mathrm{d}\mathbf{U}}{\mathrm{d}p}=\mathbf{K}^{-1}(\mathbf{p})\left(\frac{\mathrm{d}\mathbf{Q}}{\mathrm{d}p}-\frac{\mathrm{d}\mathbf{K}}{\mathrm{d}p}\mathbf{U}(\mathbf{p})\right) \tag{18}$$

leading to the adjoint form of the sensitivity equation:

$$ (p)\left(\mathbf{U}(p)\right) = \mathbf{\Lambda}^T\left(\quad)\right) \tag{19}$$

where, using the symmetric property of $\mathbf{K}$, the adjoint matrix satisfies

$$ \tag{20}$$

Unlike the aerodynamic systems of equations, Eq. (15) and (20) are usually solved efficiently using direct parallel sparse multifrontal algorithms, see [16].

2.2 Extension to an aeroelastic problem

For an aeroelastic system the state vector is defined as and the objective function is of the form $\mathcal{J}$ J( ). Design parameters $\mathbf{p}$ are linked to structural properties, $\mathbf{p}$ control the aerodynamic shape and global variables $\mathbf{p}$ affect simultaneously stiffness and shape. The design parameter vector is denoted as $\mathbf{p}$). The vector of state equations reads

$$ (\mathbf{R} \quad)) \tag{21}$$

Direct differentiation of Eq. (21) wrt. gives

$$ \frac{}{\partial \mathbf{W}} \quad \frac{}{\partial \mathbf{U}} \quad \frac{}{\mathrm{d}\mathbf{p}} \quad \frac{}{\partial \mathbf{X}_s}\frac{}{\mathrm{d}\mathbf{p}} \tag{22}$$

and solving for allows the computation of the objective function gradient

$$ \mathcal{J} \quad \mathrm{J} \quad \mathrm{J} \quad \mathrm{J} \tag{23}$$

The two blocks in Eq. (22) are coupled through aerodynamic loads applied on the structural skin, which induce an elastic deformation which in turn alters fluid grid positions.

A suitable transferring technique is applied to to compute structural loads of the form

$$ \tag{24}$$

The reference aerodynamic mesh $\mathbf{X}_{\mathrm{a}0}$ aligned with the unloaded configuration (i.e. the jig-mesh) has been introduced. This distinction is useless for the structural mesh which always matches the jig-shape. $\mathbf{T}_{surf}$ denotes the linear load transfer operator. Knowing updated structural grid positions from displacements $\mathbf{U}$, it is possible to transfer them back as $\delta\mathbf{X}$ on the aeroelastic interface through the linear splining step

$$\delta\mathbf{X}_{a,surf} = \delta\mathbf{X}_{a,surf}(\mathbf{X}_{a0}, \mathbf{X}_s, \mathbf{U}) = \mathbf{T}^U_{surf}(\mathbf{X}_{a0}, \mathbf{X}_s)\mathbf{U} \tag{25}$$

Once again, the linear displacement transfer operator $\mathbf{T}^U_{surf}$ only depends on reference meshes. Finally the fluid interior domain deformation is attained in a second step by propagating the surface deformation with

$$\mathbf{X}_a = \mathbf{X}_{a0} + \delta\mathbf{X}_a(\delta\mathbf{X}_{a,surf}, \mathbf{X}_{a0}) = \mathbf{X}_{a0} + \mathbf{T}_{vol}(\mathbf{X}_{a0})\delta\mathbf{X}_{a,surf} \tag{26}$$

where the volumic operator $\mathbf{T}_{vol}(\mathbf{X}_{a0})$ merely depends on the reference aerodynamic mesh.

Thanks to Eq. (24) through (26) it is possible to expand Eq. (22) and (23) in terms of unknown vectors $\mathrm{d}\mathbf{W}/\mathrm{d}\mathbf{p}$ and $\mathrm{d}\mathbf{U}/\mathrm{d}\mathbf{p}$. Firstly Eq. (26) is linearized wrt. $\mathbf{p}$ to give

$$\frac{\mathrm{d}\mathbf{X}_a}{\mathrm{d}\mathbf{p}} = \frac{\mathrm{d}\mathbf{X}_{a0}}{\mathrm{d}\mathbf{p}} + \mathbf{T}_{vol}\frac{\mathrm{d}\delta\mathbf{X}_{a,surf}}{\mathrm{d}\mathbf{p}} + \frac{\partial\delta\mathbf{X}_a}{\partial\mathbf{X}_{a0}}\frac{\mathrm{d}\mathbf{X}_{a0}}{\mathrm{d}\mathbf{p}} \tag{27}$$

From Eq. (25) the total derivative of the boundary displacement field is written as

$$\frac{\mathrm{d}\delta\mathbf{X}_{a,surf}}{\mathrm{d}\mathbf{p}} = \frac{\partial\delta\mathbf{X}_{a,surf}}{\partial\mathbf{X}_{a0}}\frac{\mathrm{d}\mathbf{X}_{a0}}{\mathrm{d}\mathbf{p}} + \mathbf{T}^U_{surf}\frac{\mathrm{d}\mathbf{U}}{\mathrm{d}\mathbf{p}} + \frac{\partial\delta\mathbf{X}_{a,surf}}{\partial\mathbf{X}_{s0}}\frac{\mathrm{d}\mathbf{X}_s}{\mathrm{d}\mathbf{p}} \tag{28}$$

Substituting for $\mathrm{d}\mathbf{X}_a/\mathrm{d}\mathbf{p}$ and $\partial\delta\mathbf{X}_{a,surf}/\,\partial\mathbf{p}$ from Eq. (27) and (28) into Eq. (23) leads to the following expanded form of the objective function:

$$\begin{aligned}\frac{\mathrm{d}J}{\mathrm{d}\mathbf{p}} &= \frac{\partial J}{\partial\mathbf{Y}}\frac{\mathrm{d}\mathbf{Y}}{\mathrm{d}\mathbf{p}} \\ &+ \frac{\partial J}{\partial\mathbf{X}_a}\left[\left(\mathbf{I} + \frac{\partial\delta\mathbf{X}_a}{\partial\mathbf{X}_{a0}} + \mathbf{T}_{vol}\frac{\partial\delta\mathbf{X}_{a,surf}}{\partial\mathbf{X}_{a0}}\right)\frac{\mathrm{d}\mathbf{X}_{a0}}{\mathrm{d}\mathbf{p}} + \mathbf{T}_{vol}\left(\mathbf{T}^U_{surf}\frac{d\mathbf{U}}{d\mathbf{p}} + \frac{\partial\delta\mathbf{X}_{a,surf}}{\partial\mathbf{X}_s}\frac{\mathrm{d}\mathbf{X}_s}{\mathrm{d}\mathbf{p}}\right)\right]\end{aligned} \tag{29}$$

Terms $\partial J/\,\partial\mathbf{Y}$ and $\partial J/\,\partial\mathbf{X}_a$ only depend on the equilibrium steady state and are calculated analytically in a pre-processing step. Grid sensitivity terms $\mathrm{d}\mathbf{X}_{a0}/\mathrm{d}\mathbf{p}$ and $\mathrm{d}\mathbf{X}_s/\mathrm{d}\mathbf{p}$ represent the geometric parameterization which is also part of an external dedicated procedure. Other terms like $\mathbf{T}^U_{surf}$ and $\mathbf{T}_{vol}$ and their associated partial derivatives are related to the transfer techniques used during the aeroelastic steady state computation.

By performing similar algebra manipulations, the discrete block system in Eq. (22) can be cast into the compact form

$$\begin{cases}\dfrac{\partial\mathbf{R}_a}{\partial\mathbf{W}}\dfrac{\mathrm{d}\mathbf{W}^{(\mathrm{k}+1)}}{\mathrm{d}\mathbf{p}} = -\dfrac{\partial\mathbf{R}_a}{\partial\mathbf{X}_a}\left([\mathbf{A}]\dfrac{\mathrm{d}\mathbf{U}^{(\mathrm{k})}}{\mathrm{d}\mathbf{p}} + [\mathbf{B}]\dfrac{\partial\mathbf{X}_{a0}}{\partial\mathbf{p}} + [\mathbf{F}]\dfrac{\partial\mathbf{X}_s}{\partial\mathbf{p}}\right) \\ \mathbf{K}\dfrac{\mathrm{d}\mathbf{U}^{(k+1)}}{\mathrm{d}\mathbf{p}} = [\mathbf{C}]\dfrac{\mathrm{d}\mathbf{W}^{(\mathrm{k}+1)}}{\mathrm{d}\mathbf{p}} + [\mathbf{D}]\dfrac{\mathrm{d}\mathbf{U}^{(\mathrm{k})}}{\mathrm{d}\mathbf{p}} + [\mathbf{E}]\dfrac{\partial\mathbf{X}_{a0}}{\partial\mathbf{p}} + [\mathbf{G}]\dfrac{\partial\mathbf{X}_s}{\partial\mathbf{p}} - [\mathbf{H}]\mathbf{U}\end{cases} \tag{30}$$

Constant matrices [**A**], …, [**H**] are defined analytically with the following formulas

$$
\begin{aligned}
[\mathbf{A}] &= \mathbf{T}_{vol}\mathbf{T}^{U}_{surf} & [\mathbf{B}] &= \mathbf{I} + \frac{\partial \delta \mathbf{X}_a}{\partial \mathbf{X}_{a0}} + \mathbf{T}_{vol}\frac{\partial \delta \mathbf{X}_{a,surf}}{\partial \mathbf{X}_{a0}} \\
[\mathbf{C}] &= \mathbf{T}^{Q}_{surf}\frac{\partial \mathbf{Q}_a}{\partial \mathbf{W}} & [\mathbf{D}] &= [\mathbf{M}][\mathbf{A}] \\
[\mathbf{E}] &= [\mathbf{M}][\mathbf{B}] + \frac{\partial \mathbf{Q}_s}{\partial \mathbf{X}_{a0}} & [\mathbf{F}] &= \mathbf{T}_{vol}\frac{\partial \delta \mathbf{X}_{a,surf}}{\partial \mathbf{X}_s} \\
[\mathbf{G}] &= [\mathbf{M}][\mathbf{F}] + \frac{\partial \mathbf{Q}_s}{\partial \mathbf{X}_s} & [\mathbf{H}] &= \frac{\partial \mathbf{K}}{\partial \mathbf{p}}
\end{aligned}
\tag{31}
$$

where the utility matrix $\mathbf{M} = \mathbf{T}^{Q}_{surf}\,\partial \mathbf{Q}_a / \partial \mathbf{X}_a$ has been introduced.

The system in Eq. (30) is presented in a form suitable for an iterative block scheme resolution similar to the lagged-block strategy formerly proposed in [17, 18], superscript k being the current iteration number.

Following the same notations Eq. (29) becomes

$$
\frac{\mathrm{d}J}{\mathrm{d}\mathbf{p}} = \frac{\partial J}{\partial \mathbf{Y}}\frac{\mathrm{d}\mathbf{Y}}{\mathrm{d}\mathbf{p}} + \frac{\partial J}{\partial \mathbf{X}_a}\left([\mathbf{A}]\frac{\mathrm{d}\mathbf{U}}{\mathrm{d}\mathbf{p}} + [\mathbf{B}]\frac{\partial \mathbf{X}_{a0}}{\partial \mathbf{p}} + [\mathbf{F}]\frac{\partial \mathbf{X}_s}{\partial \mathbf{p}}\right) \tag{32}
$$

Yet again, for each residual state equation in Eq. (21) an adjoint vector is introduced which multiplies the linearization of that equation, and used to formulate the augmented objective function derivative such that for any vector $\mathbf{\Lambda}_a$ and $\mathbf{\Lambda}_s$

$$
\frac{dJ}{d\mathbf{p}} = \frac{\partial J}{\partial \mathbf{Y}}\frac{\mathrm{d}\mathbf{Y}}{\mathrm{d}\mathbf{p}} + \frac{\partial J}{\partial \mathbf{X}_a}\left([\mathbf{A}]\frac{\mathrm{d}\mathbf{U}}{\mathrm{d}\mathbf{p}} + [\mathbf{B}]\frac{\partial \mathbf{X}_{a0}}{\partial \mathbf{p}} + [\mathbf{F}]\frac{\partial \mathbf{X}_s}{\partial \mathbf{p}}\right) + \mathbf{\Lambda}_a^T\frac{\mathrm{d}\mathbf{R}_a}{\mathrm{d}\mathbf{p}} + \mathbf{\Lambda}_s^T\frac{\mathrm{d}\mathbf{R}_s}{\mathrm{d}\mathbf{p}} \tag{33}
$$

Expanding $\mathrm{d}\mathbf{R}_a/\mathrm{d}\mathbf{p}$ and $\mathrm{d}\mathbf{R}_\mathbf{s}/\mathrm{d}\mathbf{p}$ and factorizing out the difficult terms $d\mathbf{U}/d\mathbf{p}$ et $d\mathbf{W}/d\mathbf{p}$ yields

$$
\begin{aligned}
\frac{\mathrm{d}J}{\mathrm{d}\mathbf{p}} &= \left(\frac{\partial J}{\partial \mathbf{W}} + \mathbf{\Lambda}_a^T\frac{\partial \mathbf{R}_a}{\partial \mathbf{W}} - \mathbf{\Lambda}_s^T[\mathbf{C}]\right)\frac{\mathrm{d}\mathbf{W}}{\mathrm{d}\mathbf{p}} + \left(\frac{\partial J}{\partial \mathbf{X}_a}[\mathbf{A}] + \mathbf{\Lambda}_a^T\frac{\partial \mathbf{R}_a}{\partial \mathbf{X}_a}[\mathbf{A}] + \mathbf{\Lambda}_s^T(\mathbf{K} - [\mathbf{D}])\right)\frac{\mathrm{d}\mathbf{U}}{\mathrm{d}\mathbf{p}} \\
&+ \frac{\partial J}{\partial \mathbf{X}_a}\left([\mathbf{B}]\frac{\partial \mathbf{X}_{a0}}{\partial \mathbf{p}} + [\mathbf{F}]\frac{\partial \mathbf{X}_s}{\partial \mathbf{p}}\right) \\
&+ \mathbf{\Lambda}_a^T\frac{\partial \mathbf{R}_a}{\partial \mathbf{X}_a}\left([\mathbf{B}]\frac{\partial \mathbf{X}_{a0}}{\partial \mathbf{p}} + [\mathbf{F}]\frac{\partial \mathbf{X}_s}{\partial \mathbf{p}}\right) - \mathbf{\Lambda}_s^T\left([\mathbf{E}]\frac{\partial \mathbf{X}_{a0}}{\partial \mathbf{p}} + [\mathbf{G}]\frac{\partial \mathbf{X}_s}{\partial \mathbf{p}} + [\mathbf{H}]\mathbf{U}\right)
\end{aligned}
\tag{34}
$$

where adjoint vectors $\mathbf{\Lambda}_a$ and $\mathbf{\Lambda}_s$ are chosen such that the following system is satisfied:

$$
\begin{bmatrix}
\left[\frac{\partial \mathbf{R}_a}{\partial \mathbf{W}}\right]^T & -[\mathbf{C}]^T \\
[\mathbf{A}]^T\left[\frac{\partial \mathbf{R}_a}{\partial \mathbf{X}_a}\right]^T & \mathbf{K}^T - [\mathbf{D}]^T
\end{bmatrix}
\begin{pmatrix}
\mathbf{\Lambda}_a \\
\mathbf{\Lambda}_s
\end{pmatrix} =
\begin{pmatrix}
-\left[\frac{\partial J}{\partial \mathbf{W}}\right]^T \\
-[\mathbf{A}]^T\left[\frac{\partial J}{\partial \mathbf{X}_a}\right]^T
\end{pmatrix}
\tag{35}
$$

Finally, once adjoint unknowns are determined, the total gradient is obtained with

$$\frac{\mathrm{dJ}}{\mathrm{d}\mathbf{p}} = \frac{\partial J}{\partial \mathbf{X}_a}\left([\mathbf{B}]\frac{\partial \mathbf{X}_{a0}}{\partial \mathbf{p}} + [\mathbf{F}]\frac{\partial \mathbf{X}_s}{\partial \mathbf{p}}\right) + \boldsymbol{\Lambda}_a^T \frac{\partial \mathbf{R}_a}{\partial \mathbf{X}_a}\left([\mathbf{B}]\frac{\partial \mathbf{X}_{a0}}{\partial \mathbf{p}} + [\mathbf{F}]\frac{\partial \mathbf{X}_s}{\partial \mathbf{p}}\right) - \boldsymbol{\Lambda}_s^T\left([\mathbf{E}]\frac{\partial \mathbf{X}_{a0}}{\partial \mathbf{p}} + [\mathbf{G}]\frac{\partial \mathbf{X}_s}{\partial \mathbf{p}} + [\mathbf{H}]\mathbf{U}\right) \tag{36}$$

3 GRADIENT COMPUTATION FOR AERODYNAMIC SHAPE OPTIMIZATION

The different test cases for inviscid and viscous flow are based on the ONERA M6 wing which has been extensively used for three-dimensional transonic CFD validation purposes, see [19].

3.1 Aeroelastic analysis and design models

The computational structured meshes depicted in Figure 1 contain 1.11 million cells divided into five blocks for the Euler grid and 3.8 million cells divided into 42 blocks for the Navier-stokes grid.

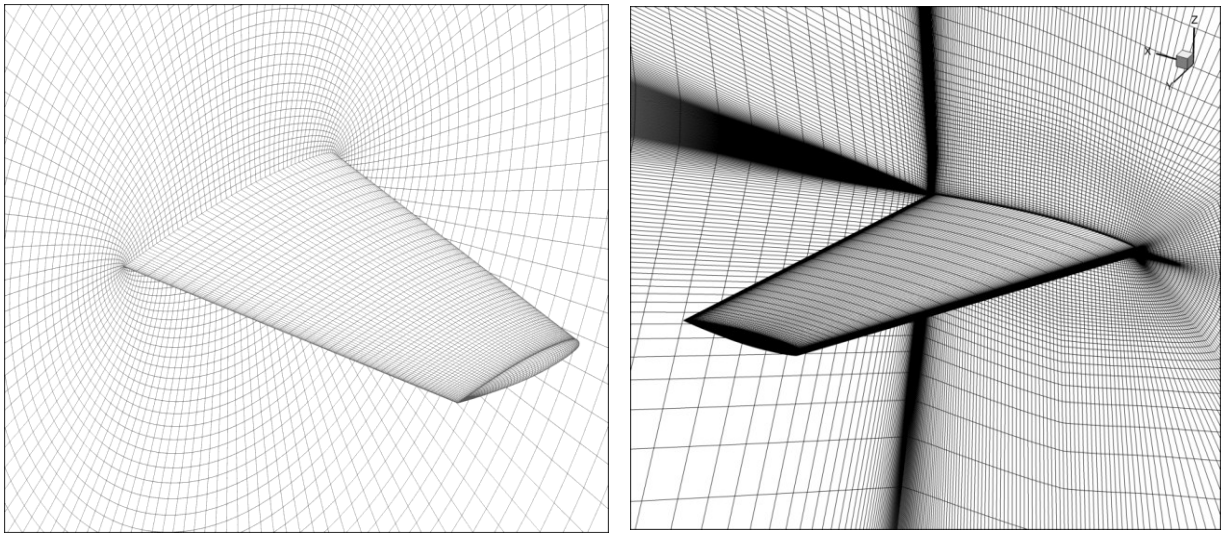

Figure 1: M6 wing Euler and RANS mesh.

The finite element model has a classical wing box layout with spars, ribs and stiffeners. Member thicknesses and sections have been designed in a pre-processing optimization step. This model can be easily tuned in order to control flexibility and consequently aeroelastic effects.

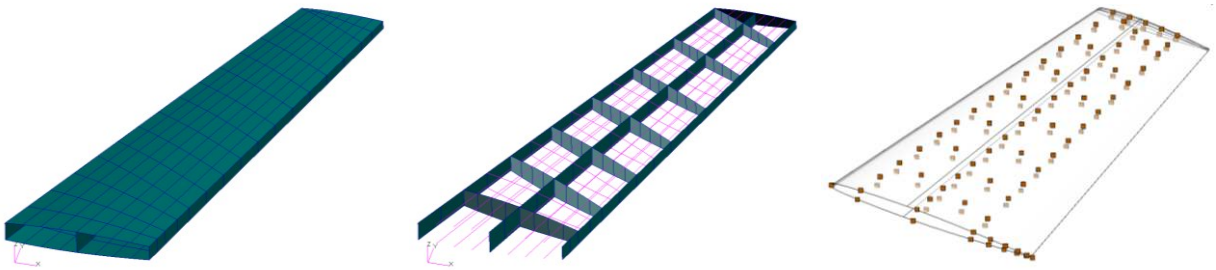

Figure 2: M6 wing structural mesh and selected displacement/force nodes for flexibility matrix construction.

The Mach number for this case is M=0.734 and the incidence is 2.08°. The wing tip displacement is 6.27cm (i.e. 5.14% of span) and the associated lift coefficient is C_z=0.196 compared to a rigid coefficient of C_z=0.221. An upwind Roe scheme with a MUSCL interpolation associated to a Van Albada limiting function is applied. The Spalart-Allmaras turbulence model has been selected.

Figure 3 below shows the pressure distribution at equilibrium and the residual norm convergence for density and turbulent variables. A first step of 600 fluid iterations is performed followed by a coupling every 200 iterations. The aeroelastic simulation exhibits an excellent convergence up to machine precision. The idea is to ensure as much as possible the cancellation of the residual that is the basic assumption for accurate discrete gradient computations.

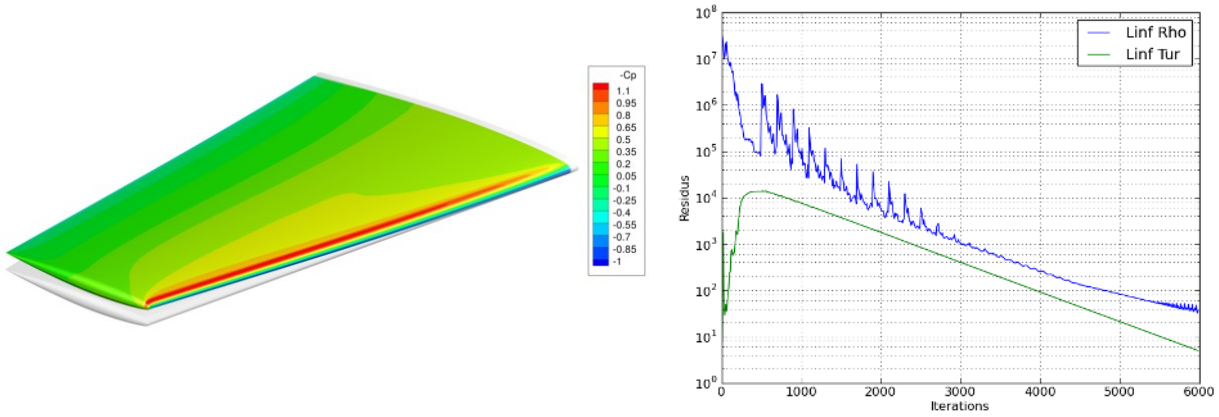

Figure 3: Cp distribution (left), convergence of density and turbulence residual norm for RANS aeroelastic simulation (right).

Three design parameters have been defined for specific assessment of gradient accuracy. First parameter x_{01} controls the section camber at 50% span and affects linearly the region from root to 90% of wing span. Second parameter x_{02} is the quarter chord twist angle at the wing tip section, and the last parameter x_{03} is the angle of attack.

3.2 Inviscid flow – Euler computations

Two gradient computations have been carried out in tangent and adjoint mode for the Euler test case. The objective is to compute total gradients for lift and pressure drag coefficients wrt. the three design parameters previously defined. The convergence of the discrete residual norm of the fluid block equations is reported in Figure 4. In direct mode, three right hand sides are considered, i.e. one for each design parameter whereas only two right hand sides are considered in adjoint mode, i.e. one for each objective function. In both direct and adjoint mode an excellent convergence is reached.

Table 1 summarizes the gradient values and allows a comparison with rigid results and finite differences. It is worth noting that flexibility effects dramatically change rigid gradient values and even reverse the sign of the drag sensitivity wrt. the camber parameter. One can observe a residual duality gap between direct and adjoint results. This is because some geometrical terms are still approximately linearized in the adjoint formulation. These approximations are currently being removed.

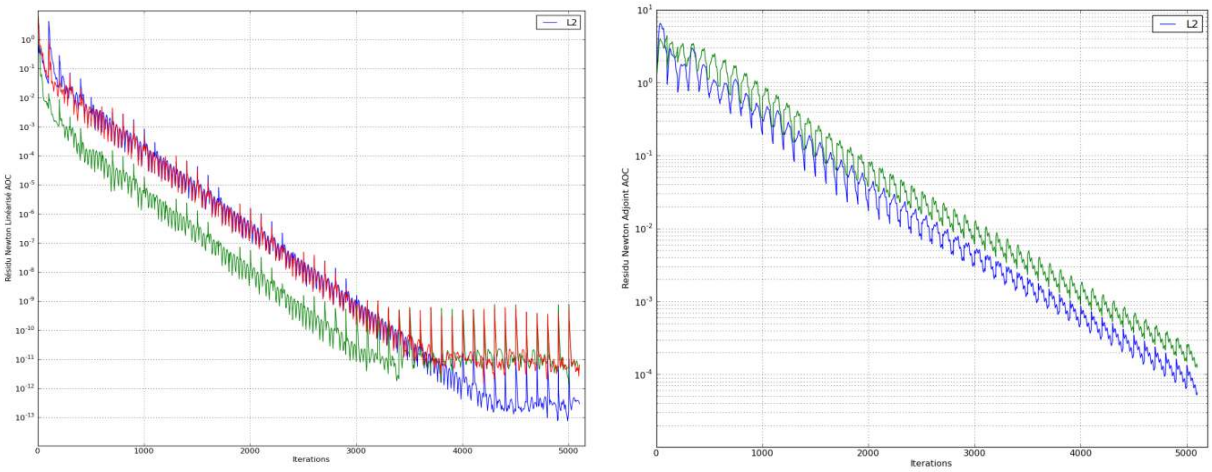

Figure 4: Convergence of linear density residual norm for three parameters (left) and adjoint density residual norm for two objective functions (right).

dC_L/dp	Rigid Adjoint	FD	Flex. Tangent	Flex. Adjoint
x_{01}	+1.56e+00	+8.13e-01	+8.141e-01	+8.057e-01
x_{02}	+5.95e-03	+8.51e-04	+8.539e-04	+9.688e-04
x_{03}	+1.30e-01	+7.13e-02	+7.142e-02	+6.943e-02

dC_{Dp}/dp	Rigid Adjoint	FD	Flex. Tangent	Flex. Adjoint
x_{01}	+1.92e-01	-1.30e-02	-1.415e-02	-1.900e-02
x_{02}	+2.85e-04	+5.62e-05	+5.648e-05	+5.367e-05
x_{03}	+1.14e-02	+3.37e-03	+3.386e-03	+3.000e-03

Table 1: Euler gradients for lift and pressure drag coefficients wrt. camber (x_{01}), tip twist (x_{02}) and angle of attack (x_{03}). Comparison between rigid, finite difference and flexible gradients in tangent and adjoint mode.

3.2.1 Viscous flow - RANS computations

The same transonic flow conditions M=0.734 and α=2.08° have been retained for the viscous test case.

Figure 5 presents the convergence histories for the density residual in tangent mode. All computations have been performed using a constant eddy and turbulent viscosity, i.e. using the standard "frozen μ_t approximation". Gradient values are summarized in Table 2 and can be directly compared with Euler values in Table 1. Obviously viscous effects significantly alter inviscid gradient values even changing the sign of the lift coefficient derivative with respect to the camber design variable. Finite difference values compare quite well with tangent results. Currently, the viscous adjoint mode is still in a validation phase and we were not able to provide reference results for the M6 wing in this paper.

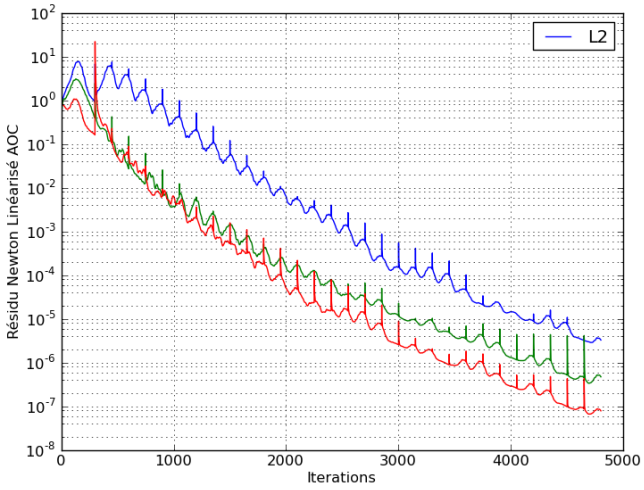

Figure 5: Convergence of linear gradient density residual for three parameters.

dC_L/dp	Rigid Adjoint	FD	Flex. Tangent
x_{01}	+1,437e+00	-6,48e-01	-6.760e-01
x_{02}	+1,950e-02	+1,90e-02	+1.844e-02
x_{03}	+7,350e-02	+6,60e-02	+6.661e-02

dC_{Dp}/dp	Rigid Adjoint	FD	Flex. Tangent
x_{01}	+5,24e-02	-4,41e-02	-4.707e-02
x_{02}	+9,05e-04	+7,18e-04	+7.240e-04
x_{03}	+3,81e-03	+2,73e-03	+2.786e-03

Table 2: Navier-Stokes gradients for lift and pressure drag coefficients wrt. camber (x_{01}), tip twist (x_{02}) and angle of attack (x_{03}). Comparison between rigid, finite difference and flexible gradients in tangent mode.

4 GRADIENT COMPUTATION FOR STRUCTURAL SIZING

The adjoint approach developed in section three is efficient whenever a reduced number of responses is considered compared to a large set of design parameters. Typically for an aerodynamic design dedicated to performance improvement, drag components and lift coefficient gradients for several flight points might be needed [20, 21]. The set of design parameters for controlling a wing shape will not exceed a few hundreds. Unlikely, structural sizing for certification has to consider failure criteria at many locations under a large set of load cases. Typically an industrial wing box sizing for preliminary design considers up to several hundreds of design parameters and up to several tens of thousands of constraints. Nonetheless, in order to still benefit from the elegant adjoint formulation, some authors have proposed a constraint aggregation approach as an attempt to reduce the size of the set of admissible constraints, and thus the number of gradients to compute. However, this technique has several drawbacks and may lead to sub-optimal designs.

Instead we propose a gradient reconstruction based on a modal approach. This technique allows a complete decoupling of the structure and aerodynamic blocks. The idea stems from the (frequency) linearized Euler or RANS solvers used in the construction of state-space models for flutter stability analysis in aeroelasticity. These solvers compute complex harmonic responses (pressure coefficients, generalized harmonic forces) to prescribed boundary displacement fields (i.e. structural mode shapes in our case).

4.1 Modal reconstruction of loads sensitivity around the steady state solution

Using previous notations, the steady equilibrium corresponding to a fluid state $\overline{\mathbf{W}}$, a mesh position $\overline{\mathbf{X}}_a$ and a structural displacement field $\mathbf{U}$ is written as

$$\mathbf{KU} = \mathbf{Q}_s = \mathbf{T}_{surf}^{Q}\mathbf{Q}_a(\overline{\mathbf{W}}, \overline{\mathbf{X}}_a) \tag{37}$$

If the full set $\mathbf{\Phi}$ of structural eigenvectors were available, the modal projection $\mathbf{U} = \mathbf{\Phi q}$ holds and then substituting in Eq. (37) gives the corresponding generalized coordinates as

$$\mathbf{q} = \boldsymbol{\gamma}^{-1}\mathbf{\Phi}^T\mathbf{Q}_s \tag{38}$$

where $\boldsymbol{\gamma} = \mathbf{\Phi}^T\mathbf{K}\,\mathbf{\Phi}$ denotes the diagonal generalized stiffness matrix.

In practice only a restricted set of first n_ϕ eigensolutions is computed and the modal approximation to $\mathbf{U}$ becomes

$$\mathbf{U} \simeq \mathbf{U}_\Phi = \sum_{i=1}^{n_\phi} \Phi_i q_i = \mathbf{K}_\Phi^{-1}\mathbf{Q}_s \text{ with } \mathbf{K}_\Phi^{-1} = \sum_{i=1}^{n_\phi} \frac{1}{\gamma_i}\Phi_i\Phi_i^T \tag{39}$$

However, remind that $\mathbf{U}$ is computed exactly from Eq. (37) such that the residual term in Eq. (39) is known from the simple difference $\mathbf{U}_{res} = \mathbf{U} - \mathbf{U}_\Phi$. Now Eq. (37) can be reformulated as

$$\mathbf{K}(\mathbf{U}_\Phi + \mathbf{U}_{res}) = \mathbf{Q}_s \tag{40}$$

Pre-multiplying this equation by $\mathbf{\Phi}^T$, then substituting for $\mathbf{U}_\Phi$ and subsequently differentiating wrt. a single design parameter p gives

$$\frac{\partial \boldsymbol{\gamma}}{\partial p}\mathbf{q} + \boldsymbol{\gamma}\frac{\mathrm{d}\mathbf{q}}{\mathrm{d}p} + \frac{\partial \mathbf{\Phi}^T}{\partial p}\,\mathbf{K}\mathbf{U}_{res} = \mathbf{\Phi}^T\frac{\mathrm{d}\mathbf{Q}_s}{\mathrm{d}p} + \frac{\partial \mathbf{\Phi}^T}{\partial p}\,\mathbf{Q}_s \tag{41}$$

In the above expression it is assumed that the sensitivity of the residual load vector is zero. This makes sense if the residual vector is thought of being an assumed deformation under a prescribed static load thus leading to $\partial(\mathbf{KU}_{res})/\partial p = 0$.

From linearized Euler or Navier-Stokes equations theory, see for instance [22, 23], it is possible to introduce a suitable first order approximation to the aerodynamic loads $\mathbf{Q}_a(\overline{\mathbf{W}}, \overline{\mathbf{X}}_a)$ in terms of a small perturbation $(\delta\mathbf{W}, \delta\mathbf{X})$ of the steady state equilibrium.

Recalling that only design parameters linked to physical properties are considered here, the system in Eq. (30) simplifies to

$$\begin{cases} \dfrac{\partial \mathbf{R}_a}{\partial \mathbf{W}}\dfrac{\mathrm{d}\mathbf{W}}{\mathrm{d}p} = -\dfrac{\partial \mathbf{R}_a}{\partial \mathbf{X}_a}[\mathbf{A}]\dfrac{\mathrm{d}\mathbf{U}}{\mathrm{d}p} \\ \mathbf{K}\dfrac{\mathrm{d}\mathbf{U}}{\mathrm{d}p} = [\mathbf{C}]\dfrac{\mathrm{d}\mathbf{W}}{\mathrm{d}p} + [\mathbf{D}]\dfrac{\mathrm{d}\mathbf{U}}{\mathrm{d}p} - \dfrac{\partial \mathbf{K}}{\partial p}\mathbf{U} \end{cases} \tag{42}$$

Solving for from the first block of equations and then substituting in the structural block gives the following system for the displacement derivatives

$$\left(\quad -[\mathbf{C}]\left[\quad\right] \quad [\mathbf{A}] + [\mathbf{D}] \right. \tag{43}$$

Now direct differentiation of Eq. (37) yields

$$\quad \quad \quad \tag{44}$$

and from direct comparison with the first block in Eq. (43) the gradient of structural loads takes the simple form

$$\quad \quad \tag{45}$$

Inserting the modal decomposition of in this expression leads to

$$\quad \mathbf{Z}\left(\mathbf{\Phi} \quad \mathbf{q}\right) \quad \tag{46}$$

In order to exploit this relation, the gradient of the generalized coordinates has to be determined first. This is done by inserting Eq. (46) into Eq. (41) to obtain

$$\quad [\boldsymbol{\gamma} \quad \mathbf{GAF}]^{-1}\left(\quad \quad \quad \quad \right) \tag{47}$$

where the generalized aerodynamic forces matrix is defined as $\mathbf{Z\Phi}$.

This equation can be simplified further if we introduce the additional assumption that design parameters only affect the stiffness matrix, i.e. $\partial\mathbf{M}/\partial p = 0$, $\mathbf{M}$ being the mass matrix. Then assuming that eigenmodes are mass-normalized, the following property is easily demonstrated

$$\tag{48}$$

Recognizing that $\mathbf{q}$, then the first term in brackets in the right hand side of Eq. (47) vanishes. Finally the expression for reads

$$\quad [\boldsymbol{\gamma} \quad \mathbf{GAF}]^{-1}\left(\mathbf{\Phi} \quad \quad \quad \right) \tag{49}$$

The residual vector gradient is approximated from the usual static sensitivity equation

$$\frac{\partial \mathbf{U}_{res}}{\partial p} = -\mathbf{K}^{-1}\left(\frac{\partial \mathbf{K}}{\partial p}\mathbf{U}_{res}\right) \tag{50}$$

To summarize the proposed strategy for the gradient reconstruction of aerodynamic forces, each vector $\mathrm{d}\mathbf{Q}_a/\mathrm{d}p$ requires at least $n_\phi + 1$ linearized rigid aerodynamic responses: n_ϕ responses to mode shapes plus one response to the generalized vector $\delta\Phi_q = (\partial\mathbf{\Phi}/\partial p)\,\mathbf{q}$. It is possible to reduce this cost to n_ϕ linearized simulations by taking advantage of the work by Wang in [24], who proposed an accurate approximation of an eigenvector derivative that is assumed to be spanned by a truncated set of normal modes augmented by a residual static mode such that

$$\frac{\partial \Phi_k}{\partial p} = \sum_{i=1}^{n_\phi} \Phi_i c_i + \Phi_{k,res} = \mathbf{\Phi c}_k + \Phi_{k,res} \tag{51}$$

where

$$\mathrm{c}_k = -\frac{1}{2}\Phi_k^T \frac{\partial \mathbf{M}}{\partial p}\Phi_k \text{ and } \mathrm{c}_{i,i\neq k} = -\frac{\Phi_i^T \frac{\partial \mathbf{L}_k}{\partial p}\Phi_k}{\lambda_\mathrm{i} - \lambda_\mathrm{k}} \tag{52}$$

and the pseudo-load matrix $\mathbf{L}_k = \mathbf{K} - \boldsymbol{\lambda}_k\mathbf{M}$. Note that in this case $\mathrm{c}_k = 0$ under previous assumption $\partial\mathbf{M}/\partial p = 0$. If a sufficient number of retained modes is considered, then the residual term becomes negligible and the linearized aerodynamic response is readily obtained from a linear combination of already available responses to mode shapes.

4.2 Aeroelastic analysis and design models

The structural and Euler fluid meshes have already been presented in Figure 2, but the Mach number for this case is M=0.83 and the incidence is 3.0°. Only an inviscid Euler flow is considered here. The wing tip displacement is 9.13 cm (i.e. 7.48% of span) and the associated lift coefficient is C_z=0.232. The steady aeroelastic computation uses an upwind Roe scheme with a Van Albada limiter. The time scheme is a Backward-Euler, with a classical pseudo time step. The density residual convergence history is presented in the figure below along with the pressure coefficient distribution at equilibrium.

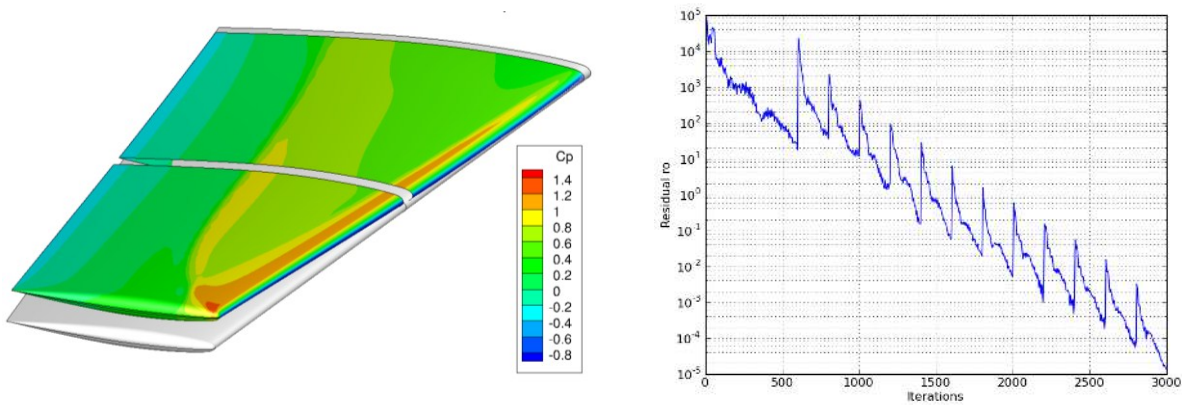

Figure 6 : Aeroelastic equilibrium shape colored by pressure coefficient (left). History of density residual norm during the fixed-point aeroelastic computation (right)

The first aeroelastic coupling is done at iteration n. 600, then the coupling operation repeats every 200 iterations, for a total number of 3000 iterations.

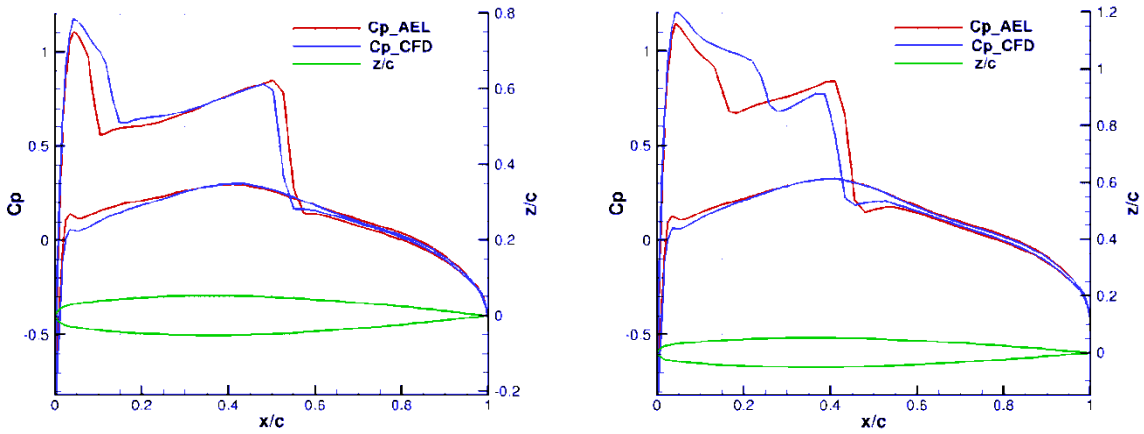

Figure 7 : Comparison between rigid and flexible Cp distribution at section y=50% and y=75% span.

Two design parameters have been defined for the structural model. First parameter p_1 controls the thickness of the linked lower and upper skin, and second parameter p_2 affects the thickness of the spar webs. Finally, the smoothed mode shapes used to approximate the structural displacements are presented in Figure 9.

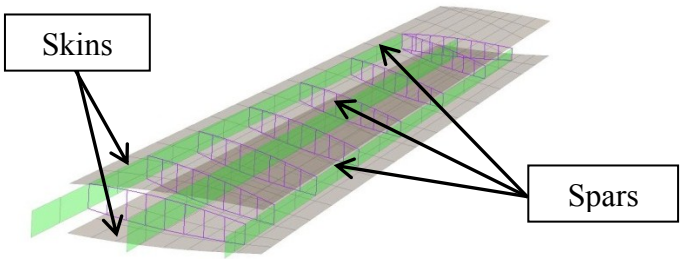

Figure 8 : Structural design parameters.

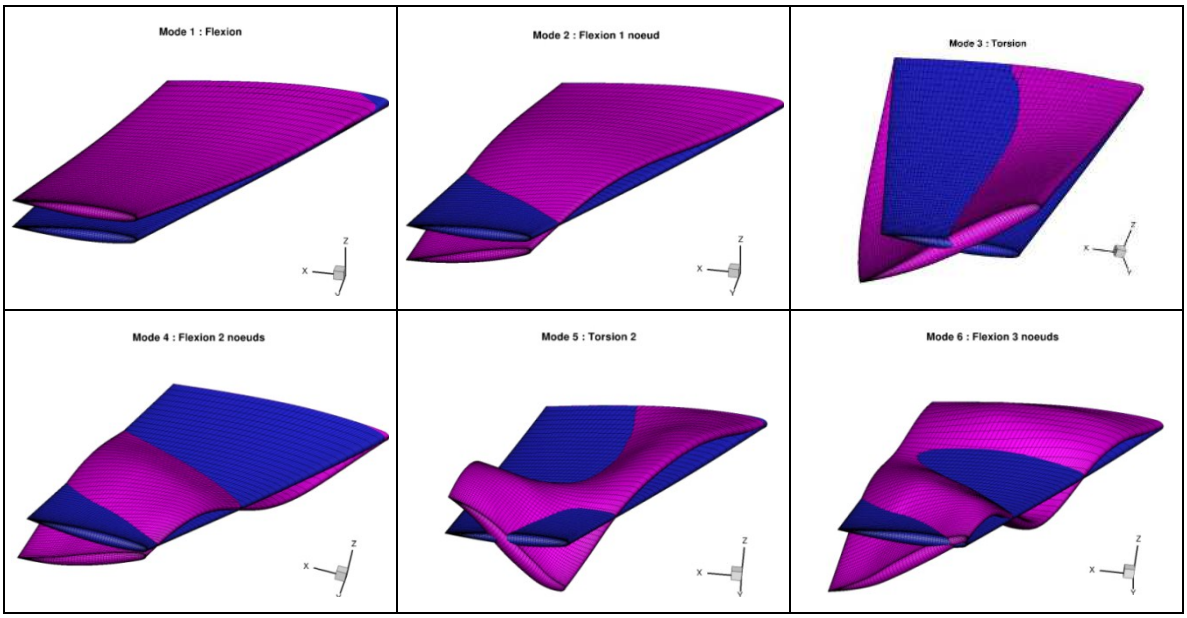

Figure 9 : First six structural mode splined on the wetted surface.

4.3 Gradient computation and results

Figure 10 and Figure 11 represent the results obtained respectively for the reconstruction of the pressure coefficient gradient w.r.t first and second design parameter, compared with the gradients obtained by finite difference method.

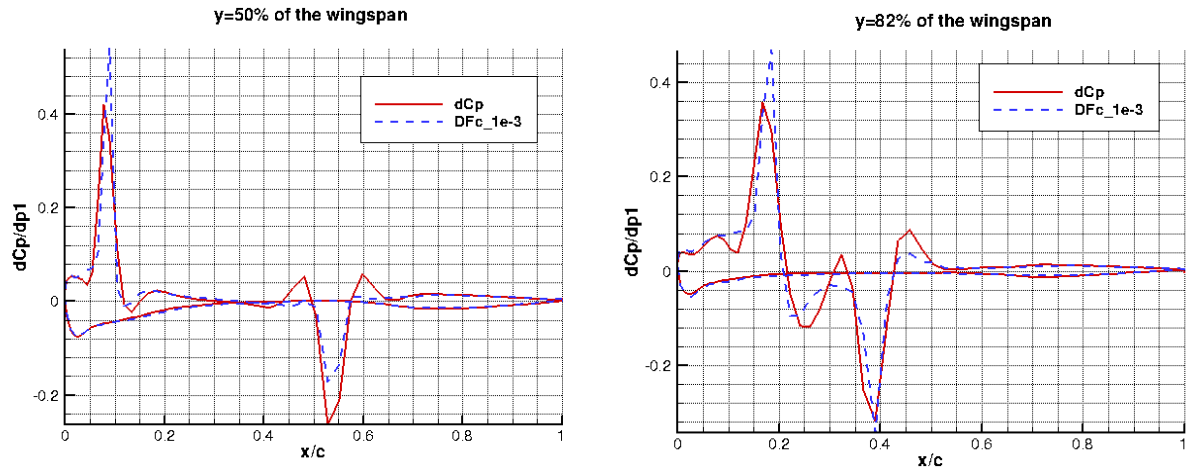

Figure 10 : Reconstruction of the pressure coefficient gradient wrt. p_1 compared to finite differences (dashes).

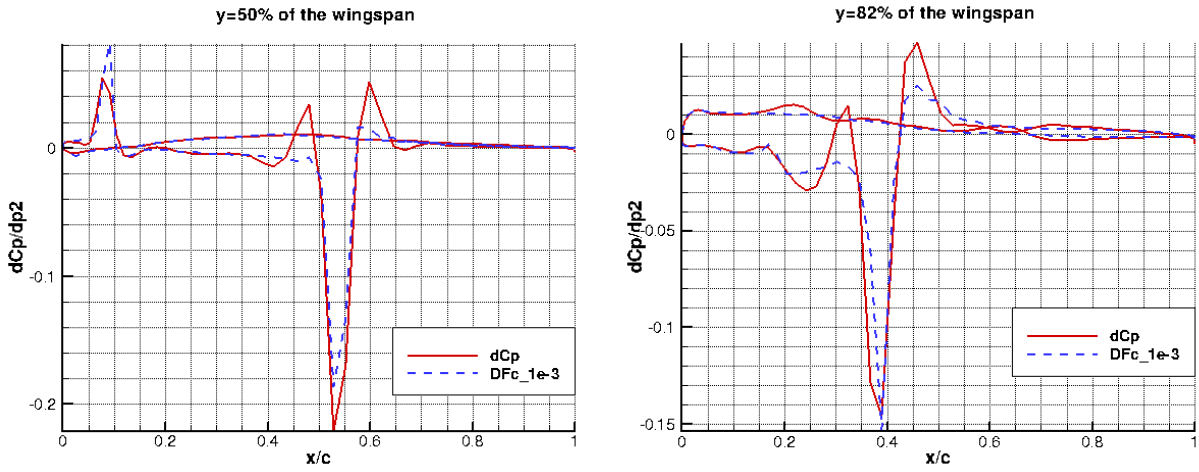

Figure 11 : Reconstruction of the pressure coefficient gradient wrt. p_2 compared to finite differences (dashes).

For both parameters the reconstruction is very close to the finite difference results, which validates the linearized approach proposed in this study. In order to reduce the number of computations, the accuracy of the gradient reconstruction is assessed without the contribution of eigenvector derivatives in Eq. (46) and (49). Corresponding results are presented in Figure 12 for parameter p_2. Table 3 below summarizes the reconstructed gradients for lift coefficient.

$\mathrm{d}C_L/\mathrm{d}p$	FD (Ael)	$\boldsymbol{\Phi}$, $\partial\boldsymbol{\Phi}/\partial p$	$\boldsymbol{\Phi}$
p_1	-1.85E-02	-1.68E-02	-2.08E-02
p_2	+7.01E-03	+7.52E-03	+8.65E-03

Table 3 : Gradients for lift coefficient wrt. wing skin and spar thickness. Values with and without eigenvector derivatives contribution. Reference finite difference values are provided.

Obviously, this reconstruction is of less quality which points out the relevant contribution of eigenvector derivatives.

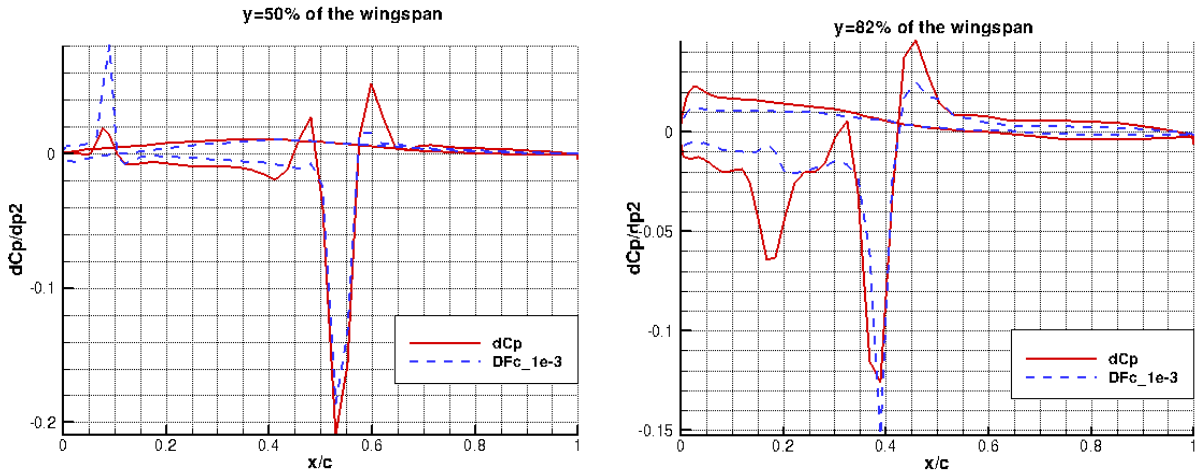

Figure 12 : Reconstruction of the pressure gradient wrt. second design parameter compared to finite difference computation, without eigenvector derivatives contribution

In order to understand the relevancy of adding eigenvector derivatives to the equations, the distance between subspaces spanned by the eigenvectors and their derivatives has been calculated. As these subspaces are of the same dimension, the Grassmann distance using the principal angles can be computed [25] to give:

p_1	p_2
0.479	0.493

Table 4 : Relative Grassmann distance between subspaces spanned by eigenvectors and eigenvector derivatives wrt. skin thickness p_1 and spar web thickness p_2.

The relative Grassmann distance (i.e. normalized by maximum value) for p_1 is less than the one for p_2. This means that the information provided by the eigenvector derivatives is more useful in the latter case than in the former.

5 CONCLUSION

The ***elsA*** block-structured highly scalable software has been enriched with a new capability for aeroelastic gradient computation for aerodynamic shape optimization. This new module is no more restricted to simplified structural models and benefits from the highly parallel architecture of ***elsA***. Theoretical details of the proposed direct and adjoint formulation are provided as well as numerical preliminary results for the M6 wing test case for inviscid and viscous fluid models. Thanks to advanced relaxation and acceleration techniques, excellent convergence rates have been observed.

In addition, a non-intrusive modal approach is proposed to obtain an accurate reconstruction of gradients with respect to structural stiffness parameters. This technique only requires harmonic responses to prescribed boundary displacements on the wetted area and benefits from the existing linearized Euler or RANS solvers used in the construction of state-space models for flutter stability analysis in aeroelasticity. Results for an inviscid transonic test case are reported for the M6 wing.

Additional complex 3D geometry aircraft applications such as wing-body and complete aircraft are currently being considered to assess the full potentiality of the new module and will be reported elsewhere. Further developments will extend the embedded aeroelastic gradient module to support structural design parameters as well.

6 REFERENCES

[1] Blondeau C., Irisarri F-X, Leroy F-H., Salah El Din I., "A Bi-Level High Fidelity Aero-Structural Integrated Design Methodology - A Focus on the Structural Sizing Process," *RAeS 3rd Aircraft Structural Design Conference*, Delft, The Netherlands, 9-11th October 2012.

[2] Salah El Din I., Dumont A., Blondeau C., "Transonic Wing-body Civil Transport Aircraft Aero-Structural Design Optimization using a Bi-Level High Fidelity Approach – A Focus on the Aerodynamic Process", *51st AIAA ASM*, Grapevine, Texas, 2013.

[3] Cambier L., Veuillot J.-P., "Status of the elsA Software for Flow Simulation and Multi-Disciplinary Applications", 46th AIAA *Aerospace Sciences Meeting and Exhibit*, Reno, Nevada, Jan. 2008.

[4] Girodroux-Lavigne P., "Recent Navier-Stokes aeroelastic simulations using the elsA code for aircraft applications", *International Forum on Aeroelasticity and Structural Dynamics*, 18-20 June 2007, Stockholm, Sweden.

[5] Marcelet M., Peter J., Carrier G., "Sensitivity Analysis of a Strongly Coupled System Using the Discrete Direct and Adjoint Approach", *Revue Européenne de mécanique numérique*, Vol. 17, 1077-1106, 2008.

[6] Dumont A., Ghazlane I. , Marcelet M., Carrier C., Salah El Din I., "Overview of Recent Development of Aeroelastic Adjoint Method for Civil Aircraft Wing Optimization", *ONERA DLR Aerospace Symposium*, February 2011.

[7] Ghazlane I., Carrier G., Marcelet M., Dumont A., "Aerostructural Adjoint Method for Flexible Wing Optimization", *8th AIAA MDO Specialist Conference*, AIAA-2012-1924.

[8] Mavriplis D. J., "A Discrete Adjoint-Based Approach for Optimization Problems on Three-Dimensional Unstructured Meshes", AIAA-2006-0050.

[9] Nielsen E.J., Anderson W.K., "Recent Improvements in Aerodynamic Design Optimization on Unstructured Meshes", *AIAA Journal*, Vol. 40, No. 6., pp.1155–1163, 2002.

[10] Fazzolari, A., Gauger N., Brezillon J., "Efficient aerodynamic shape optimization in MDO context", *Journal of Computational and Applied Mathematics*, Vol. 203, pp. 548-560, 2007.

[11] Kenway G.K.W., Kennedy G.J., and Martins J. R. R. A., "Scalable Parallel Approach for High-Fidelity Steady-State Aeroelastic Analysis and Adjoint Derivative Computations", *AIAA Journal*, 52(5):935-951, 2014.

[12] Gauger N., "Efficient Deterministic Approaches for Aerodynamic Shape Optimization", in *Optimization and Computational Fluid Dynamics*, Chapter 5, Springer-Verlag, 2008.

[13] Peter J., Dwight R.P., "Numerical sensitivity analysis for aerodynamic optimization: A survey of approaches". *Computer and Fluids,* Vol. 39, pp. 373-391, 2010.

[14] Peter, J., Drullion,F., "Large Stencil Viscous Flux Linearization for the Simulation of 3D Compressible Turbulent Flows with Backward-Euler Schemes", *Computer and Fluids*, Vol.36, pp.1005–1027, 2007.

[15] Nielsen E.J., Lu J., Park M. A., Darmofal D. L., "An implicit, exact dual adjoint solution method for turbulent flows on unstructured grids", *Computers and Fluids*, Vol. 33, pp. 1131–1155, 2004.

[16] Amestoy P.R., Duff I.S., l'Excellent J.-Y., "Multifrontal parallel distributed symmetric and unsymmetric solvers". *Computer Methods in Applied Mechanics and Engineering* 184 (2–4): 501–520, 2000.
[17] Martins J., "A coupled adjoint method for high-fidelity aero-structural optimization", Phd, Stanford University CA, November 2000.
[18] Maute K., Nikbay M., Farhat C., "Coupled analytical sensitivity analysis and optimization of three-dimensional nonlinear aeroelastic systems", *AIAA Journal*, 39(11), 2001.
[19] Schmitt, V. and Charpin, F., "Pressure Distributions on the ONERA M6 Wing at Transonic Mach Numbers", *Experimental Data Base for Computer Program Assessment*, AGARD Advisory Report AR-138, May 1979.
[20] Gallard F., Meaux M., Montagnac M., Mohammadi B., "Aerodynamic aircraft design for mission performance by multipoint optimization", proceedings of the *21st AIAA applied CFD conference*, San Diego, USA, 2013
[21] Reuther J.J., Jameson A., Alonso J.J., Rimlinger M. J., and Saunders D., "Constrained Multipoint Aerodynamic Shape Optimization Using an Adjoint Formulation and Parallel Computers", Part 1 & 2, *Journal of Aircraft*, 36(1):51–74, 1999.
[22] Jameson A., "In Time dependent calculation using multigrid, with application to unsteady flows past airfoil and wings", June 1991.
[23] Mortchéléwicz G., "Prediction of aircraft transonic aeroelasticity by the linearised Euler equations", 41st Israël Annual Conference on Aerospace Sciences, Tel-Aviv, 2001.
[24] Wang B.P., "Improved approximate methods for computing eigenvector derivatives in structural dynamics", *AIAA Journal*, Vol. 29, No. 6, pp. 1018-1020, 1990.
[25] Hamm J., Lee Daniel D., "Grassmann Discriminant Analysis: A Unifying View on Subspace-Based Learning", *25th International Conference on Machine Learning*, 2008.

7 ACKNOWLEDGEMENTS

The authors wish to thank Airbus Group for partially funded this work. We also address many thanks to Antoine Dumont from the Applied Aerodynamics Dept. for providing the aerodynamic meshes, shape parameterization inputs and finite difference results. We also greatly appreciated fruitful discussions with Jacques Peter from the Computational Fluid Dynamics Dept. for his knowledge of the ***elsA*** software and advices for debugging strategies.

8 COPYRIGHT STATEMENT